

SINGLE AND TWO-PHASE SODIUM FLOW ANALYSIS FOR TWO TUCOP CABRI TESTS USING THE ASTEC-Na CODE

Sara Perez-Martin, Werner Pfrang

Institute for Neutron Physics and Reactor Technology (INR)
Karlsruhe Institute of Technology (KIT)
Hermann-von-Helmholtz-Platz 1, Eggenstein-Leopoldshafen, Germany
sara.perez@kit.edu, werner.pfrang@kit.edu

Giacomino Bandini, Stefano Ederli, Paolo Balestra, Carlo Parisi

Italian Agency for New Technologies, Energy and Sustainable Economic Development (ENEA)
Via Martiri di Monte Sole, 4
Bologna, Italy
giacomino.bandini@enea.it, stefano.ederli@enea.it, paolo.balestra@enea.it, carlo.parisi@enea.it

ABSTRACT

The development and validation of ASTEC-Na code as a safety code system for severe accident analysis is being performed in the framework of the JASMIN project supported by the European Commission. One of the main tasks of the modelling and validation tasks of this project is devoted to the sodium thermal hydraulic behavior both in single and two-phase regimes. In this paper we present the first ASTEC-Na results of E8 and EFM1 in-pile tests conducted in the CABRI experimental reactor. These two tests are LOF+TOP transients. We present for both CABRI tests a comparison between experimental data and ASTEC-Na results for transient coolant temperatures at different heights, boiling onset time, inlet and outlet flow rate and the evolution of the sodium two-phase front during the boiling time up to TOP onset. Besides, a benchmark is presented comparing ASTEC-Na simulation results with the results of other safety codes such as CATHARE, RELAP5-3D and SAS-SFR.

KEYWORDS

ASTEC-Na, two-phase sodium, FBR, severe accidents, code benchmarking

1 INTRODUCTION

The design of future nuclear reactors with high safety standards needs as a fundamental tool, robust, validated computational simulation code that can predict fuel pin behaviour, thermo-hydraulics, the global core behaviour and evaluate the source term under any type of possible accidental conditions. Code system development and validation require adequate experiments covering the various interfering physical processes and phenomena at different scales to assess the accuracy of different code models. In Unprotected Loss of Flow (ULOF) type accidents in a Sodium-cooled Fast Reactor (SFR), single-phase and two-phase sodium behaviour has an important influence on the accident scenario through phenomena such as the sodium void reactivity feedback which could initiate a power transient. Therefore it is required that the sodium thermal-hydraulics model in any simulation code gives an adequate prediction of boiling onset, evolution of the voiding zone, clad dry-out, clad motion onset and fuel pin break-up conditions. This is also necessary for providing precise initial and boundary conditions for subsequent accident phases.

The JASMIN project of the 7th European Framework Programme aims at developing a new computer code system, ASTEC-Na, capable of evaluating the consequences of protected and unprotected accidents

in a Sodium-cooled Fast Reactor [Ref. 1, 2]. ASTEC-Na is based on the ASTEC code system, jointly developed by IRSN and GRS, extensively validated through European projects in FP5, FP6 and FP7 for LWR. One of the four modelling and validation tasks of this project focuses specifically on the sodium thermal-hydraulics behaviour [Ref. 3]. The validation and verification of ASTEC-Na thermal-hydraulic models is being performed through the analysis of adequate in-pile single-pin experiments of the CABRI programs, and fuel rod-bundle experiments of the SCARABEE program. Furthermore, the results from the natural circulation test conducted in the French sodium-cooled reactor PHENIX have been extensively used for validation purposes. Additionally, some of the tests to be carried out in the KASOLA sodium loop (in advanced state of construction at KIT/Karlsruhe) will be investigated [Ref. 4, 5]. The validation of ASTEC-Na is planned to be complemented by several code benchmarking activities using more system codes like: SAS-SFR, CATHARE, RELAP5-3D, RELAP5-Na and SIMMER-III, so that insights into more advanced modelling approaches than those currently implemented in ASTEC-Na could be adopted from these codes.

CABRI experiments were selected from the test matrix defined for the overall code validation, as representative of both single- and two-phase flow regimes. These tests are the ones characterized by the Loss Of Flow (LOF) and eventually followed by an overpower transient (TOP). Among the available CABRI tests, the pure LOF B11 test and the LOF+TOP E8 and EFM1 tests have been considered for validation and benchmarking purposes. In this paper we present the work performed in the analysis of the initial loss of flow phase of E8 and EFM1 tests where we have assessed the following thermal-hydraulics models: clad to coolant heat transfer, pressure drop correlations, boiling onset and two-phase flow dynamics.

2 ASTEC-NA THERMAL-HYDRAULICS MODELS

CESAR is the thermal-hydraulics module of ASTEC-Na [Ref. 6, 7]. This module is particularly important because it provides boundary conditions to other modules in the code (i.e., pin module, neutronics, fission products/aerosol transport, etc.) and it also delivers input for the containment part. The thermal-hydraulic modeling of Na in a SFR has been based on the LWR version of the CESAR module [Ref. 7]. Its adaptation to the SFR environment has required not only implementing Na properties in the Material Data Bank of ASTEC, but also an update of all the expressions describing heat and mass fluxes between Na phases and between Na and component/system surfaces [Ref. 6].

The heat and mass exchanges between liquid and vapor are calculated using the kinetic theory of gases. The model considers two normal flows at the interphase: the vapor molecules hitting the surface and remaining there (i.e., condensation) and the spontaneous liquid evaporation. If vapor and liquid temperatures are identical and Na pressure is the saturation one, both flows should be equal. Two additional phenomena are considered: Na flashing, when the total pressure is lower than the liquid saturation one (i.e., liquid bulk boiling); and bulk condensation, when the Na vapor pressure is greater than the vapor saturation pressure. Beyond heat transfer associated to mass exchange, a convective mechanism between both Na phases has been also accounted for. This term might be significant in volumes which atmospheres consist massively of non-condensable gases. The formulation relies on the Newton's law of cooling where the heat transfer coefficient is estimated as the inverse function of a series coupling of the individual thermal resistances of phases: pure conduction for the dispersed phase (i.e., bubbles or droplets) and convection for the continuous one. Wall-to-fluid heat exchange largely depends on the Na phase. The phenomena modeled for liquid Na are: convection, nucleate boiling, film boiling, thermal radiation and droplet projection (i.e., heat flux from the droplets emerging from the quench front). Figure 1 displays all those heat transfer regimes in the heat flux – temperature domain. The temperature of Critical Heat Flux (T_{CHF}) is obtained through the Thom's correlation [Ref. 8] and the Critical Heat Flux (q_{CHF}) from the Zuber's correlation once corrected for liquid subcooling [Ref.9]. The Minimum Stable Film temperature (T_{MSF}) is calculated using Berenson's correlation [Ref.10]. Nevertheless, few studies are

available on wall-Na heat exchange at high wall temperature, so that these expressions seem to be highly uncertain and further investigation should be done. As for convection, several options are given to estimate the Nusselt non-dimensional number, whereas nucleate boiling is modeled with the Forster & Zuber correlation [Ref. 11]. Radiation exchange is based on the grey-body approximation. The mean value of the Heat Transfer Coefficient in the projection region is fixed to $300 \text{ W/m}^2\text{K}$ and shows a quadratic decrease with the increasing distance from the quench front. As for wall-to-Na vapor, convection and radiation are considered. Convective heat transfer is assumed to be the maximum between natural and forced regimes (the last one estimated with the Dittus-Boelter correlation [Ref.12]).

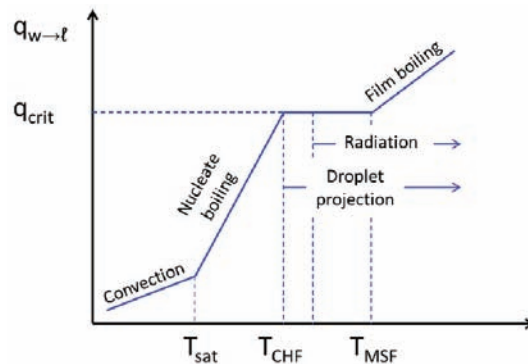


Figure 1 Wall-Na heat transfer regimes

Regarding the other codes used in this work for benchmarking, RELAP5-3D [Ref. 13, 14] is the latest code version in the series of RELAP5 codes developed at the Idaho National Laboratory (INL) for thermal-hydraulic transient analysis of LWR systems. RELAP5-3D can be used for the simulation of a wide variety of hydraulic and thermal transients in both nuclear and non-nuclear systems involving mixtures of vapor, liquid, non-condensable gases, and non-volatile solutes. The application of this code is also extended to sodium-cooled reactors. The Seban-Shimazaki correlation is used to calculate the convective heat transfer with sodium coolant. The CATHARE code [Ref. 15], jointly developed by CEA, EDF, AREVA and IRSN, was originally conceived for safety studies of PWR systems and recently extended to other nuclear reactors, particularly to sodium-cooled fast reactors. CATHARE has a flexible modular structure for thermal-hydraulic modelling in applications ranging from simple experimental test facilities to large and complex installations like nuclear power plants. The Spukinski heat transfer correlation is used for sodium in CATHARE. The SAS-SFR code [Ref. 16, 17] performs deterministic analysis for steady state power operation and accident conditions, caused by protected or unprotected loss of coolant flow or reactivity insertion in Sodium-cooled Fast Reactors, during the so-called initiation phase¹. This code is the result of a long-term international cooperation between scientists from KIT/INR (Germany), CEA, IRSN (France) and JAEA (Japan). SAS-SFR has been extensively qualified with a variety of results from various experiments. Major calculation models contained in SAS-SFR code include the steady-state fuel irradiation behavior, the transient fuel deformation behavior, the primary main coolant system heat transport, the sodium boiling model, the cladding tube melting and motion analysis, the analysis of fuel failure behavior in voided and un-voided regions. The core nuclear and heat calculation model of SAS-SFR is a multi-channel model, grouping fuel assemblies with similar nuclear and heat characteristics into a channel which is represented by a single pin. The sodium voiding model is a multiple-bubble slug ejection model that handles flow area changes and non-uniform axial nodes. It simulates the axial distribution of the voiding extent (for calculating the voiding reactivity feedback), the heat removal from the cladding surface after the onset of voiding and the vapor flow rates that drive the molten cladding motion.

¹ The phase during which the core damage is limited to fuel assemblies and the motion of the failed fuel is uniformly controlled by the wrapper tube wall.

3 COMPUTATIONAL RESULTS FOR THE TWO TUCOP TRANSIENTS

E8 consisted of a TUCOP (Transient Under Cooling Over Power) test using a fuel pin with 4.6 at.% burn-up, hollow pellets and 316 SS cladding. The fuel pin was subjected first to a LOF and then to a structured TOP leading to pin rupture in a partially voided coolant channel. The main objective of this test was to study the fuel dispersion with an annular and industrial pin subjected to a structured transient in a partially voided cooling channel. On the other hand, EFM1 was also a TUCOP test using a fuel pin with 6.4 at.% burn-up, hollow pellets and 15-15 Ti cladding where the TOP was triggered in a voided channel, about 8 s after boiling onset (BO). The aim of this test was to study the extended fuel motion in an unrestrained coolant channel using a pin with annular pellets, high burnup and upper axial blanket. As for E8 test we focused only on the first phase of the experiment that is, on the LOF transient before the TOP triggering. In E8 test this period is 22.1 s and in EFM1 is 30.7 s. Table I shows the characteristics of the E8 and EFM1 tests and the experimental results obtained. Their corresponding LOF phases show similarities in the inlet coolant temperature and the coolant heat-up. However, they have also differences in the peak linear rating, which is much larger in E8 test than in EFM1 and the nominal flow rate which is coherently larger in E8 than in EFM1.

Table I. Characteristics of the E8 and EFM1 tests

	E8	EFM1
Date	June 30 th , 1988	May 6 th , 1994
Used Fuel Pin	OPHELIE6	SCARABIX
Type of fissile pellets	Annular MOX	Annular MOX
Type of cladding	316 SS	15-15 Ti
Fuel pin burnup (at%-MWd/t.ox.)	4.9-46400	6.4-60604
PPN ² linear power at st-st (W/cm)	593	487
Sodium temp at BFC ³ (°C)	402	390
Sodium heat-up (°C)	180	182
Fissile length (cm)	76.6	76.2
Flow halving time (s)	6.5 ≤ τ ≤ 7.9	6.5 ≤ τ ≤ 8.3
Nominal Flow Rate (l/h)	676	564
Superheat (°C)	Not observed	12
Saturation temperature (°C)	976	972
Local boiling onset (s)	20.7	21.9
Local boiling duration (s)	0.1	0.8
Bulk boiling onset (s)	20.8	22.7
Fission gas release time(s)	Not observed	25.4
Clad dry-out (s)	Not observed	25.7-26.4
TOP onset after LOF onset (s)	22.1	30.7
“ “ after boiling onset (s)	1.3	8.0

ASTEC-Na modelling for E8 fuel pin considers both lower and upper fertile blankets and fission gas plena besides the fissile column. Lower and upper structures of the test section are considered as well with a total axial length of 3.10 m. CATHARE modelling considers the same regions as ASTEC-Na with 3.16 m total length. RELAP5-3D takes into account the same fuel pin regions as ASTEC-Na, but only the structure of the test section above the fuel pin is simulated. The lowest region considered is the lower fission gas plenum. The total axial length simulated is 2.86 m. SAS-SFR modelling considers the same

² PPN: Peak Power Node

³ BFC: Bottom of the Fissile Column

regions as ASTEC-Na both for the fuel pin and the structures below and above with 2.95 m as total axial height. In all calculations it was agreed to consider the BFC as the zero axial height reference. For EFM1, ASTEC-Na modelling is very similar to E8 considering the same regions. For this test all codes take into account the same test section zones.

Table II. Calculated fuel pin PPN characteristics at steady state prior to E8 and EFM1 transients onset

	Experiment	ASTEC-Na	CATHARE	RELAP5-3D	SAS-SFR
E8					
Fuel Clad Gap Width at PPN (μm)	-	66.12	66.10	66.12	0.00
Inner Fuel Radius at PPN (mm)	-	1.023	1.023	1.023	1.144
Outer Fuel Radius at PPN (mm)	-	3.719	3.719	3.719	3.854
Inner Clad Radius at PPN (mm)	-	3.786	3.786	3.786	3.854
Outer Clad Radius at PPN (mm)	-	4.366	4.366	4.366	4.445
PPN Axial Location (cm BFC)	37	36.3	38.3	37.2	38.3
Height of the Fiss. Column (cm)	76.6	76.6	76.6	76.6	76.4
Total channel power (W)	36,709	36600	36600	36600	38830
Total power produced in the fuel (%)	96.6	100	100	100	98.0
Sodium inlet temperature (K)	676	673	673	673	669
Sodium flow rate (m^3/h)	0.676	0.681	0.677	0.677	0.683
Outlet pressure (b)	-	2.38	2.38	2.38	2.38
Peak Linear Rating (W/cm)	593	611	612	626	608
EFM1					
Fuel Clad Gap Width (μm)	-	80.30	80.30	80.30	0.00
Inner Fuel Radius (mm)	-	1.036	1.036	1.036	1.234
Outer Fuel Radius (mm)	-	3.640	3.640	3.640	3.728
Inner Clad Radius (mm)	-	3.720	3.720	3.720	3.728
Outer Clad Radius (mm)	-	4.290	4.290	4.290	4.298
PPN Axial Location (cm BFC)	44	43.962	43.962	44.885	43.510
Height of the Fiss. Column (cm)	76.2	76.2	76.2	76.2	76.6
Total channel power (W)	31050	31050	31050	31050	31530
Total power produced in the fuel (%)	98.3	100	100	100	97.3
Sodium inlet temperature (K)	663	663	663	663	662
Sodium flow rate (m^3/h)	0.564	0.567	0.564	0.556	0.567
Outlet pressure (b)	-	2.22	2.22	2.22	2.24
Peak Linear Rating (W/cm)	491	504	504	513	491

The fuel and clad inner and outer radii in ASTEC-Na, CATHARE and RELAP5-3D calculations are taken from GERMINAL code calculation where the simulations of the power operation irradiation of OPHÉLIE and SCARABIX fuel pins in PHENIX reactor were performed. SAS-SFR is able to simulate power operation as well as transients, therefore the fuel and clad status prior to LOF onset is based on its previous calculations. It includes not only geometry, but fission gas retention, fuel and clad thermal and mechanical characteristics. Table II presents the calculated state of the fuel pin at the Peak Power Node

(PPN) and the steady-state conditions for E8 and EFM1 tests prior to the LOF onset. Although the gap is taken as small, only 66 μm in ASTEC-Na, it means that gap is still open in CABRI steady state. According to SAS-SFR gap is closed. As for E8 tests, ASTEC-Na, CATHARE and RELAP5-3D consider that the fuel-clad gap is open for EFM1 fuel pin, 80 μm , while for SAS-SFR the gap is closed. Figure 2 shows the coolant pressure profiles at LOF onset for E8 and EFM1 tests. The predicted reduction of coolant pressure is very similar for all codes. The Na flow coast-down for the LOF transients imposed in E8 and EFM1 experiments is plotted in Figure 3. Code calculations follow the experimental data rather good in the Na single phase for both experiments. Pink zones indicate the estimated error of the measurements, which is $\pm 4\%$.

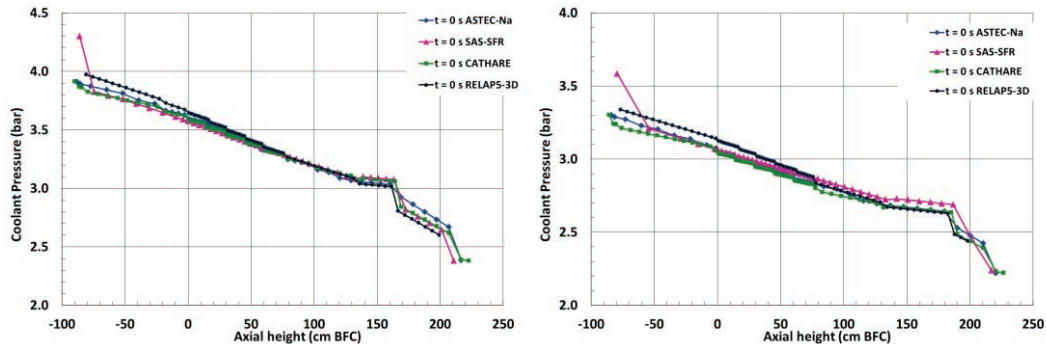


Figure 2 Coolant pressure profile in the different calculations for E8 test (left) and for EFM1 test (right)

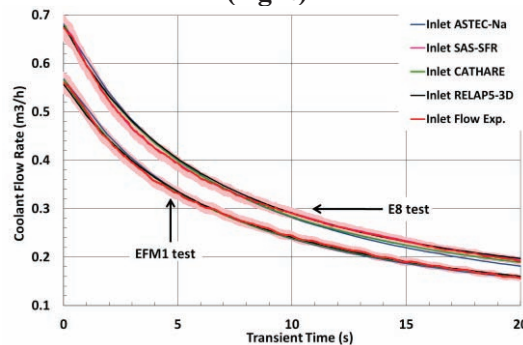


Figure 3 Comparison of coolant flow coast down in the single sodium phase for E8 and EFM1 tests

3.1 E8 test analysis

The measured evolution of the coolant temperature at different axial fuel pin heights is depicted in Figure 4. The different curves with the same color indicate that there were considerable azimuthal variations in Na temperature between thermocouples (TC) situated at the same elevation. This fact was due to pin distortion, leading to different cross sections in the coolant channel around the pin. Uncertainties in the experimental devices might also be the reason of the TC temperature differences but in a minor way since the estimated temperature error is 1.6 %. Figure 5 shows the Na temperature profiles at $t=0$ and 2 s after LOF onset. Red dots represent the experimental measurements. There was at least a pair of TC at each axial elevation. The coolant heat-up is well reproduced by all calculations in the fuel pin axial region. Above the fuel pin there are discrepancies in the code results coming from the assumptions of radial heat losses through the surrounding structures. SAS-SFR assumes that the upper structure is in thermal equilibrium with the coolant at the steady-state prior to LOF onset, so the Na temperature does not decrease. This fact is verified by the TC situated at 95 cm BFC. The maximum differences are lower than

25 K at the test section outlet. 2 s after LOF onset the coolant temperature is around 20 K larger at TFC⁴ than at steady-state. The temperature at the upper region is lower than the TFC and according to SAS-SFR results the temperature at the outlet is not modified yet. Figure 6 shows the comparison of Na temperature profiles at 6 s and 20 s after the LOF onset. The experimental measurements at the same height become closer and the code results are in very good agreement. Code results converge for the temperature in the upper region, except RELAP5-3D which predicts temperatures about 25 K larger. The behavior of the coolant in the upper part will affect the evolution of the voiding zone since the structures around the test section might act as a heat sink. In general, it can be said the calculation results are reasonable along the fissile region comparing with the experimental data in the coolant single-phase stage of the LOF transient.

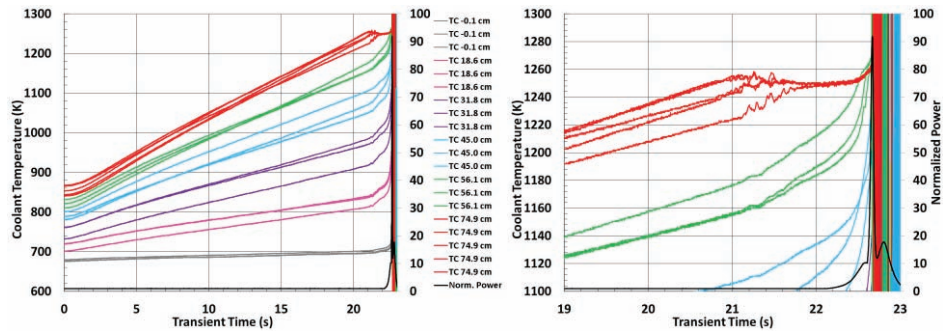


Figure 4 Coolant temperature measurements at different axial heights for E8 test

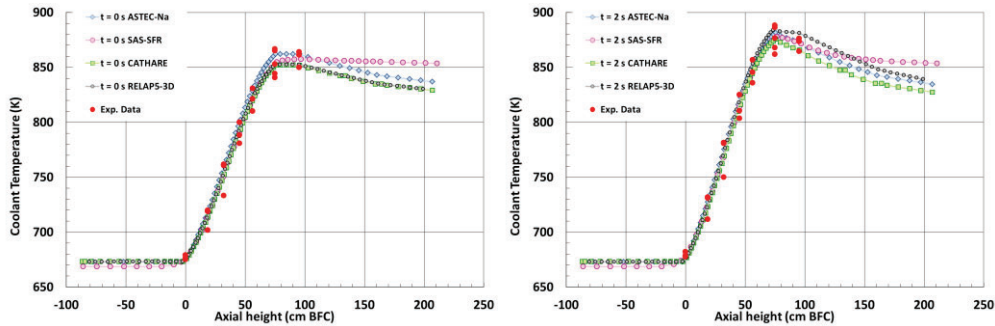


Figure 5 Coolant temperature profiles at LOF onset (left) and at t=2 s (right) for E8 test

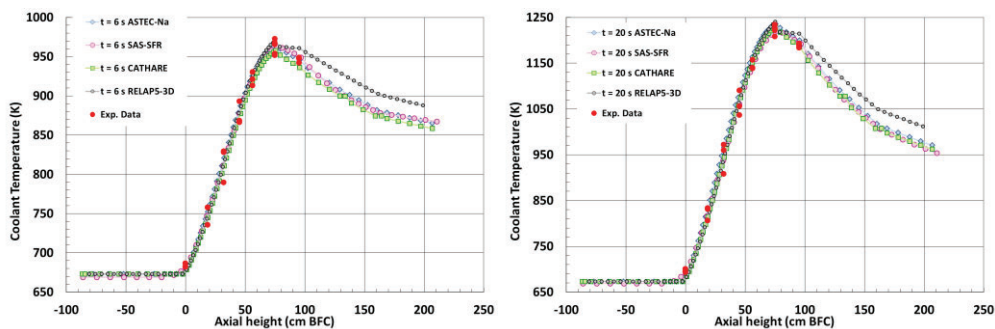


Figure 6 Coolant temperature profiles 6 s (left) and 20 s (right) after LOF onset for E8 test

After LOF triggering Na temperatures increase nearly linearly until the saturation temperature (T_{sat}) is reached at TFC at 20.7 s transient time when Local Boiling Onset (LBO) occurred. After LBO boiling spread azimuthally and the Bulk Boiling Onset (BBO) was estimated to be total at 21.4 s. The first TC reached T_{sat} at 20.7 s. However, the last TC at TFC did not approach the saturation plateau until 21.6 s.

⁴ TFC: Top of the Fissile Column

whilst the TC situated in between reached T_{sat} between 20.7 and 21.6 s. The TC signals therefore confirm that for ~ 0.9 s sodium boiling did not extend entirely around the pin. In ASTEC-Na calculation boiling onset (BO) occurs at 20.9 s that is only 220 ms delayed. The other codes predict more delayed BO times except RELAP5-3D that gets a boiling time 300 ms before the experimental value. In all cases the axial location is at TFC as it was observed experimentally. Calculated T_{sat} is in very good agreement with the measured one which indicated that the pressure boundary conditions used in the calculations are reasonable. Table III presents the calculated transient results. Bulk sodium superheat was not detected in this experiment. Neither fission gas blow out nor cladding dry-out or clad melting were detected before TOP onset because TOP was triggered during the rewetting phase. ASTEC-Na and CATHARE calculations predicts however clad dry-out 1.1 s and 1.4 s after BO, respectively.

Table III. Calculated transient results for the E8 test

	Experiment	ASTEC-Na	CATHARE	RELAP5-3D	SAS-SFR
Local boiling onset time (s)	20.7	-	-	-	-
Bulk boiling onset (s)	21.6	20.92	21.10	20.40	21.98
Boiling onset height (cm BFC)	75	75.62	75.62	69.72	79.17
Saturation temperature (K)	1250	1247.2	1246.3	1248.0	1251.0
Pressure at TFC (bar)	-	2.17	2.19	2.19	2.18
Clad dry-out time (s)	Not observ.	22.0	22.5	-	-
Clad melting onset time (s)	Not observ.	22.7	22.8	-	-

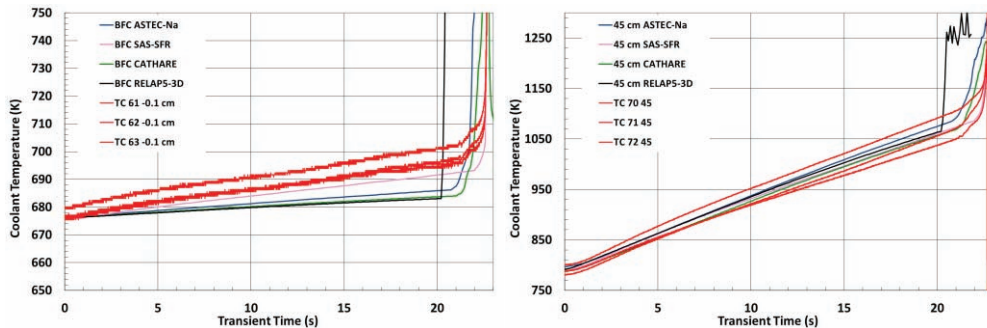


Figure 7 Coolant temperature at BFC and 45 cm BFC for E8 test

The coolant temperatures at BFC and at 45 cm BFC during the LOF transient are depicted in Figure 7. Measurements differ for about 20 K at BFC. All calculation results present a deviation in the temperature and cannot reach exactly the observed temperatures. However at 45 cm BFC the calculations are in good agreement with the measurements.

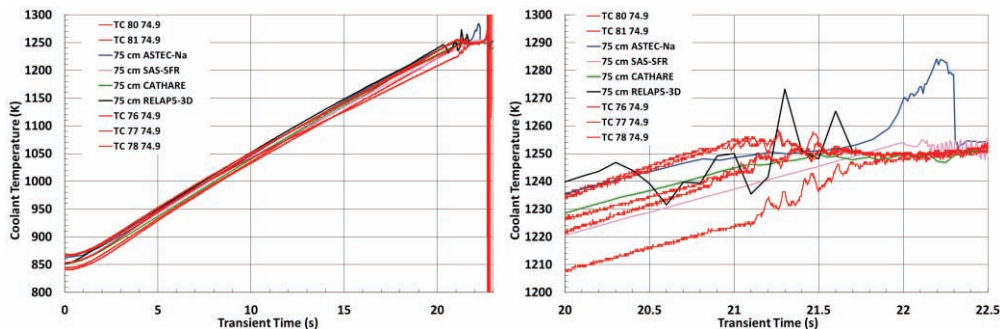


Figure 8 Coolant temperature at TFC for E8 test

Figure 8 shows the coolant temperature at TFC. Also at this height the evolution of the temperature is well simulated by all codes. On the right hand side of the Figure 8 the coolant behavior is plotted around T_{sat} . From the experimental data it can be seen that BO was local initially. Two TC reach T_{sat} first, but the others needed some more hundreds ms to get T_{sat} . The calculated T_{sat} are very similar in all cases however, the responses after BO are different. RELAP5-3D calculation cannot reproduce the smooth behavior of the experimental data but it shows a very irregular behavior before the calculation stops. The other three calculations get T_{sat} correctly as well as the stable behavior in the first seconds after boiling. ASTEC-Na calculation predicts clad dry-out at 22.0 s into the transient. At that time the coolant temperature shows a rapid temperature increase. This however cannot be observed experimentally.

In general, after boiling a high pressure increase is generated due to the big difference between liquid and vapor sodium densities. This pressure increase affects the liquid sodium around the first sodium bubbles and the sodium flow reduction generates consequently more Na bubbles. Besides, clad temperature rises since sodium vapor heat transfer coefficient is lower than that of the liquid sodium. Thank to the still flowing sodium, some bubbles condense but others are created again and for a certain period of time this bubble creation and condensation sequence is produced, establishing the so-called rewetting phase. This fact makes the flow rate oscillate due to pressure changes. The flow rate behavior is very dependent on the power and cooling conditions of the test. When BBO is well established and the flow rate can no longer absorb the heat from the clad, the sodium two-phase front starts to propagate in axial directions.

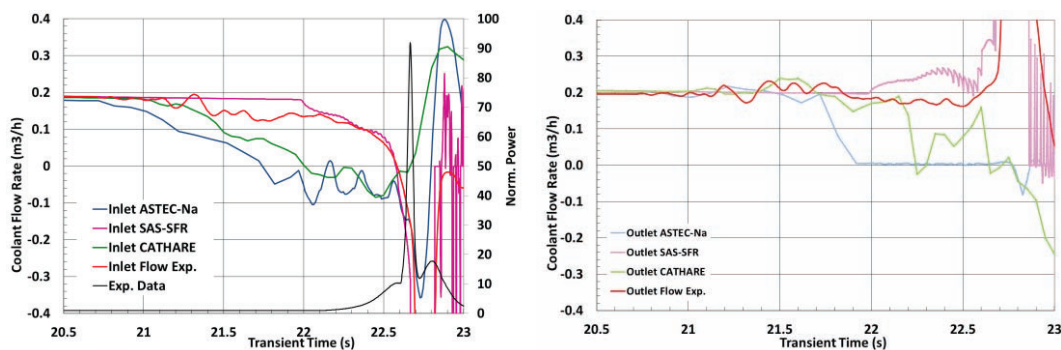


Figure 9 Inlet and outlet flow rate after boiling onset for E8 test

The inlet and outlet flow rates after boiling inception are plotted in Figure 9. The black line shows the power pulse triggered 22.1 s after LOF onset. Focusing on the time range up to TOP onset, the experimental curve presents a very smooth flow reduction with soft oscillations. ASTEC-Na and CATHARE results predict a larger flow rate decrease, however oscillation frequencies are reasonable. SAS-SFR boiling onset is very close in time to TOP onset therefore it cannot predict this stable flow phase. Nevertheless SAS-SFR follows rather well the sudden flow drop produced after the TOP triggering and gives reasonable results for the fuel response under the structured power pulse. The experimental outlet flow rate is hardly reduced completely by the codes before TOP onset. A very stable outlet flow rate with light oscillations was observed. The particular characteristics of E8 test, specially the large nominal flow rate, show that boiling can be stabilized for a few seconds. CATHARE has a right outlet flow rate response up to 22.2 s but ASTEC-Na predicts a drop of the flow rate to 0 m³/h after 21.7 s.

Inlet and outlet flow rates give an indication of the voiding volume progression (see left hand side of Figure 10). During approximately 1 s boiling was stabilized at TFC and afterwards the voiding zone is extended in both axial directions. However inlet and outlet flow rates do not vary very much, they just present some oscillations. The calculated sodium boiling interfaces can be seen on the right hand side of Figure 10. Since none of the codes can reproduce the boiling stabilization due to the difficulty to take into account the fuel pin distortion, we have moved the time axis in order all data sets to coincide in the point where the voiding region propagates axially. The calculated results are reasonable considering the time

shift except for RELAP5-3D whose lower front is overestimated. For the lower front ASTEC-Na, CATHARE and SAS-SFR are very similar. The evolution of the upper void front in ASTEC-Na results is underestimated compared to the observed one up to 600 ms bulk boiling time. The fact that the upper interface is kept constant afterwards might be correlated with the imposed heat losses (external temperature and heat transfer coefficient) in the upper part of the test section leading to strong vapor condensation. CATHARE calculation underestimates the upper front as well. It considers similar heat losses condition as ASTEC-Na, however it leads to less vapor condensation and then the upper front is higher than in ASTEC-Na. SAS-SFR shows a good agreement for both lower and upper interfaces.

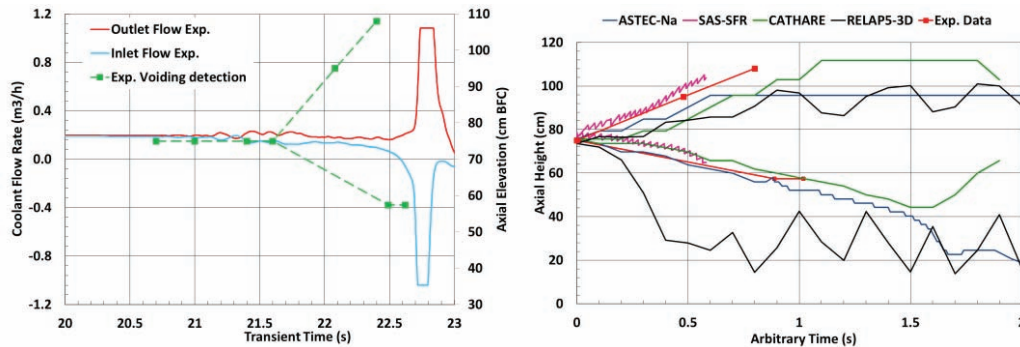


Figure 10 Experimental voiding zone (left) and calculated voiding regions (right)

3.2 EFM1 test analysis

EFM1 test had a larger LOF transient time period since TOP was triggered 30.7 s after LOF onset, thus the voiding zone was extended during 8.0 s before TOP onset. The Na temperature measurements at different axial heights are depicted in Figure 11. As for E8, differences in the TC measurement at the same elevations put in evidence the slight off-centering of the pin position in the coolant channel. The estimated temperature error is 1.6 %.

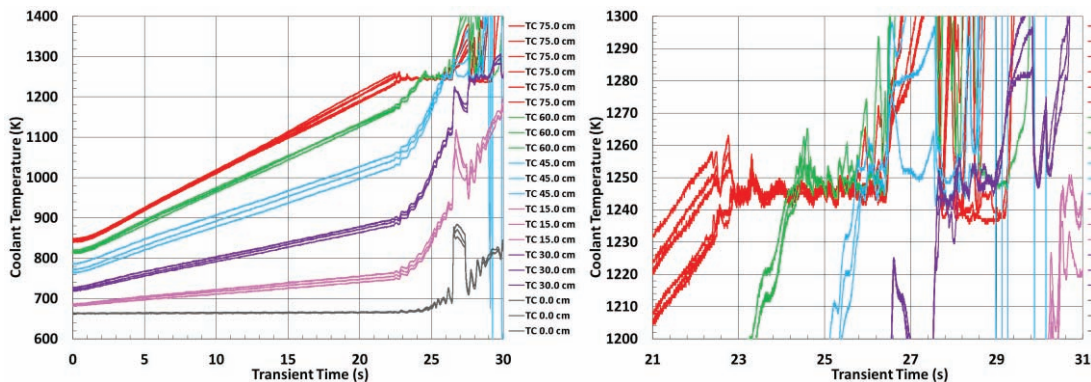


Figure 11 Coolant temperature measurements at different axial for EFM1 test

Figure 12 presents the comparison of the Na temperature profiles at $t=0$ and 2 s after LOF onset. As for E8 analysis, red dots represent the experimental measurements. The calculated coolant heat-up is similar to the experimental data in the fuel pin axial region. Nevertheless ASTEC-Na predicts a coolant temperature at TFC 7 K larger than the largest TC measurement. Above the fuel pin there are discrepancies in the code results coming from the assumptions of radial heat losses. According to measurements the uppermost part of the structure was in thermal equilibrium with the coolant. This behavior is well reproduced by SAS-SFR. The differences with the experimental data at the outlet are 20

K for ASTEC-Na, 27 K for CATHARE and 30 K for RELAP5-3D. The coolant temperature profiles at 8 s and 20 s after LOF triggering are shown in Figure 13. At 45 cm BFC the TC measurements vary about 28 K, however at other elevations the temperatures are closer (11 K at 60 cm BFC and 7 K at TFC). At TFC ASTEC-Na temperature is 17 K larger than the largest temperature measurement. At this time the Na temperature in the upper part of the test section is in better agreement than in the previous transient time shown in Figure 12. The calculated temperature decrease follows an approximate exponential decay to 850 K.

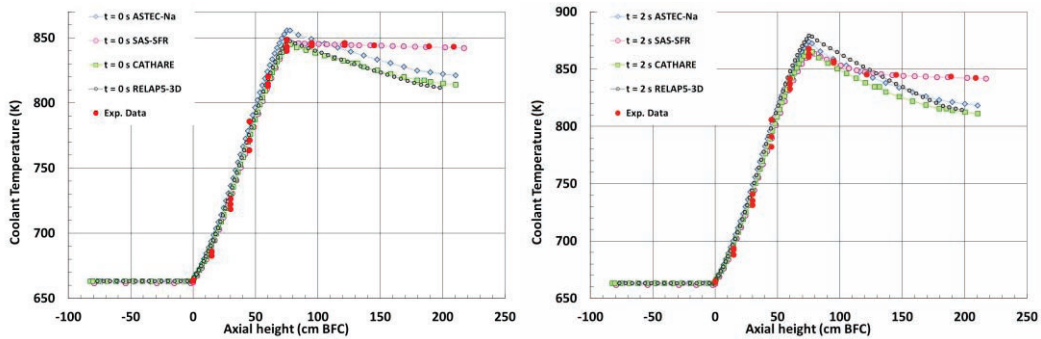


Figure 12 Coolant temperature profiles at LOF onset and 2 s after LOF onset for EFM1 test

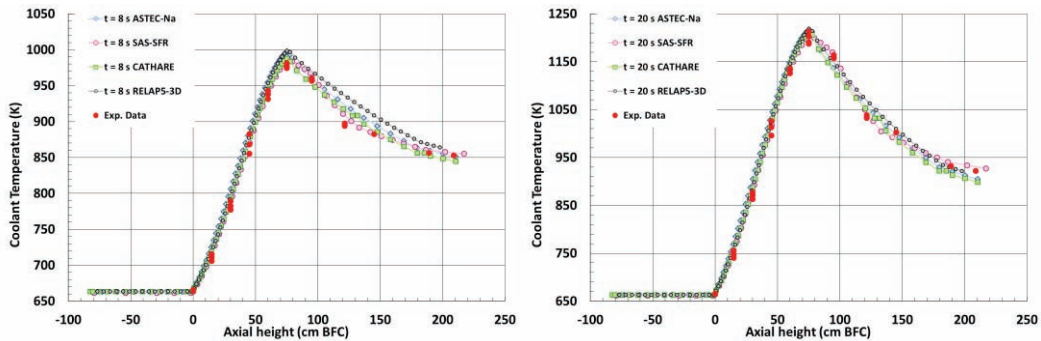


Figure 13 Coolant temperature profiles 8 s and 20 s after LOF onset for EFM1 test

Experimentally local boiling started 21.9 s after LOF onset. It was detected from the inlet and outlet flowmeter responses and from the coolant channel TC situated at TFC. The detection of boiling inception was also possible by integrating the difference between the outlet and inlet flowmeter signals indicating the voided volume produced. When analyzing the coolant temperature measurements at TFC it appears that LBO occurred at a local spot in the coolant channel cross section where the coolant was superheated locally by about 12 K (see right hand side of Figure 11). However, at BBO 800 ms later, coolant temperatures in the cross section of fissile height were equilibrated.

Table IV. Calculated transient results for the EFM1 test

	Experiment	ASTEC-Na	CATHARE	RELAP5-3D	SAS-SFR
Local boiling onset time (s)	21.9	-	-	-	-
Bulk boiling onset time (s)	22.7	21.80	21.70	21.60	22.51
Boiling onset height (cm BFC)	75	75.22	75.22	75.45	77.00
Saturation temperature (K)	1246	1242	1241	1252	1248
Pressure at TFC (bar)	-	2.09	2.10	2.27	2.12
Clad dry-out time (s)	25.7-26.4	23.00	23.5	-	25.1
Clad melting onset time (s)	-	24.70	24.7	-	26.3

In ASTEC-Na calculation boiling starts 21.8 s after LOF onset. This is just 0.1 s earlier than the experimental observed time of LBO. The other codes predict earlier boiling onset except SAS-SFR that gets 600 ms delayed boiling time compared to LBO and 200 ms earlier than BBO. In all cases the axial location is at TFC as it was observed in the experiment. The calculated T_{sat} are $-5/+6$ K around the experimental value. Table IV presents the calculated transient results.

If flow rate reduction is long enough clad dry-out might occur where even the sodium liquid film in contact with the clad is evaporated. Experimentally, between 3 and 3.7 s after bulk boiling onset temporary clad dry-out is observed at TFC and 30 cm BFC. They are small peaks before the final big temperature increase. This is the previous stage to fission gas blow-out and clad melting. Gas blow-out takes place when the integrity of the clad is compromised and the clad internal pressure due to the fission gasses in the plena and gap overtakes the mechanical clad resistance. In EFM1 test 26.4 s after the beginning of the transient, 3.73 s after BBO, flowmeter signals and pressure transducers gave clear indications for a rapid coolant channel voiding as consequence of Fission Gas Plenum Blow-out (FGPB) for a time period of ~ 300 ms. The upper part of the fuel pin remained voided for the rest of the transient but about 250 ms later the lower part of the pin started to be filled with sodium again. During rewetting of the super-heated cladding surfaces at about 1.5 s after FGPB pressure spikes were measured reaching a significant value of ~ 3 -4 bar. This was a first indication of the re-entering of sub-cooled liquid sodium reacting with very hot or even partially molten clad material. The whole event sequence of FGPB and rewetting lasted ~ 1.8 s only. This fact could mean that the fission gas inventory was small and the subsequent sodium vapor formation was not very pronounced. After the FGPB event, the lower sodium slug reached the axial pin height as before the event, therefore the subsequent boiling behavior was not very much different from the expected in a case without FGPB event. This is mainly the reason why in SAS-SFR calculation FGPB is not considered, even if it contains an option to activate such phenomena.

Figure 14 shows the Na temperature at 60 cm and 75 cm BFC. All code results are very similar in the first 21 s after LOF onset at 60 cm BFC. RELAP5-3D predicts a sudden temperature increase before the other calculations and the experimental data. ASTEC-Na and CATHARE give very similar temperature increase after boiling but slightly larger than the experimental one. SAS-SFR gives accurate results. Coolant temperatures at BFC and 30 cm BFC are shown in Figure 15. The coolant temperature increases after the FGPB due to gasses passage and it almost follows the same slope than before the blow-out. Except for the blow-out phenomena itself not used in SAS-SFR, this code presents a good agreement with the experiment for 30 cm BFC elevation. ASTEC-Na and CATHARE show a similar tendency but with larger slope. This fact should be related to the flow rate reduction after boiling onset.

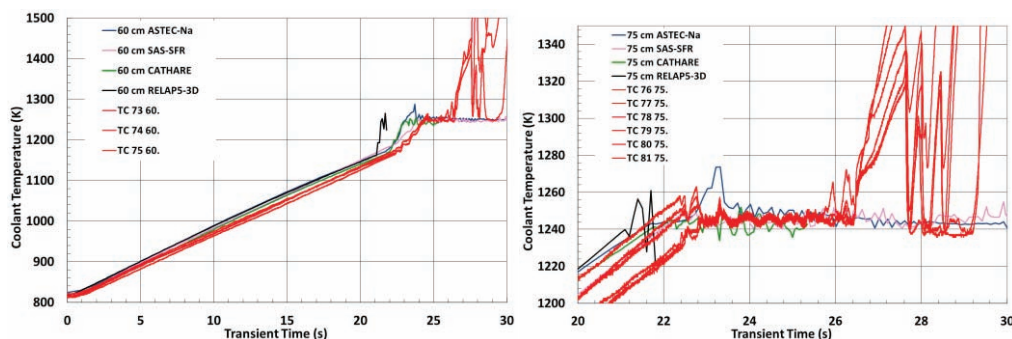


Figure 14 Coolant temperature at 60 cm and 75 cm BFC for EFM1 test

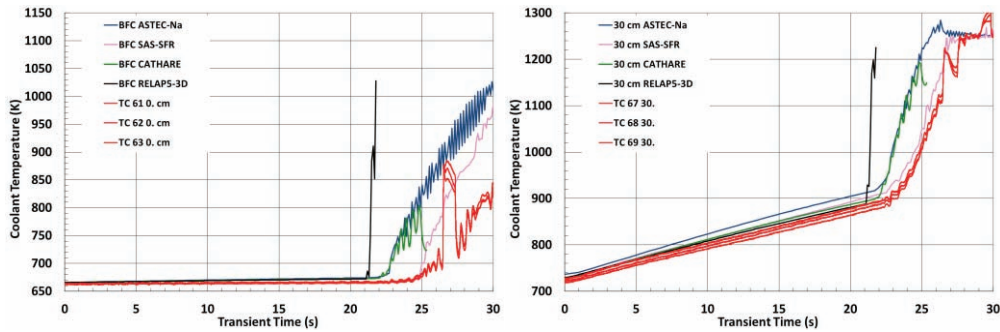


Figure 15 Coolant temperature at BFC and 30 cm BFC for EFM1 test

The evolution of the inlet flow rate and the boiling interfaces are depicted in Figure 16. Up to boiling onset the agreement is rather good, but the coolant two-phase behavior is different for ASTEC-Na and CATHARE where flow reduction is higher compared to the observed one. This fact explains the much rapid increase of coolant temperature after boiling onset in the previous figures. However oscillation frequencies are similar to experimental data. The calculated sodium boiling interfaces can be seen on right hand side of Figure 16. Experimentally the lower two-phase interphase moved downward into fissile pin height more or less regularly. ASTEC-Na lower front is reasonable but overestimates slightly the elevation. For the upper front however, ASTEC-Na prediction is very deficient, it looks like the upper front is stopped slightly above TFC. CATHARE and SAS-SFR provide a better agreement with the experiment up to 2-2.5 s boiling time; afterwards both codes underestimate the upper sodium interphase, being partly due to the not simulated FGFB.

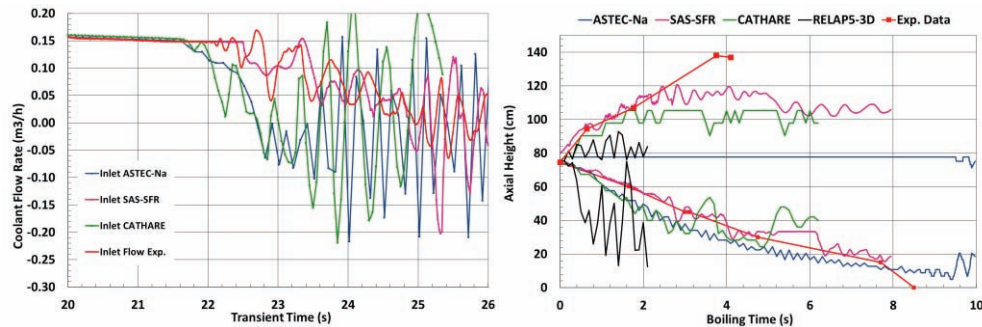


Figure 16 Inlet flow rate and the evolution of the liquid sodium fronts for EFM1 test

4 CONCLUSIONS

The analyses of two TUCOP tests using ASTEC-Na code have been presented. And a benchmarking using CATHARE, RELAP5-3D and SAS-SFR codes has been showed. We have focused our analysis on the first phase of the transients where the LOF transient is deployed prior to fuel pin failure or break-up.

For both E8 and EFM1 tests ASTEC-Na gives satisfactory results for sodium single phase. Coolant heat-up and variation of the heat-up during the single phase of the LOF transient are in good agreement with the experiments. The other codes have also a rather well response. Boiling onset is predicted by ASTEC-Na with a small difference with respect to the observed one. However, the difficulty to consider the fuel pin distortion observed during the experiment affecting strongly the local boiling inception should be mentioned. Therefore, despite of this modelling difficulty boiling onset is calculated reasonably well.

Calculated sodium two-phase flow behavior is poorer using ASTEC-Na. Inlet and outlet flow rates are underestimated in ASTEC-Na calculations after boiling onset in both E8 and EFM1 tests. The lower

voiding interface is in agreement with the experimental data for E8 and slightly underestimated for EFM1. The upper front is underestimated for both tests. The reason of those discrepancies needs to be identified by performing parametric studies on the consideration of radial heat losses and on the mass and heat transfer equations for two-phase sodium. Concerning the code benchmarking, code results differences can be attributed to differences between codes in input data, treatment of radial heat loss and pressure calculations.

ACKNOWLEDGMENTS

The authors acknowledge the European Commission of funding the JASMIN project N°295803 in FP7 in the Topic Fission-2011-2.2.1 “Support for ESNII”. Special thanks to Dr. Dankward Struwe for the technical support provided during the preparation of this work as related to KIT contribution.

REFERENCES

1. N. Girault et al “The European JASMIN project for the development of a new safety simulation code, ASTEC-Na, for Na-cooled fast neutron reactors” *Proceedings of ICAPP 2013*, Jeju island (Korea), April 14-18, 2013.
2. N. Girault et al “On-going activities in the European JASMIN project for the development and validation of ASTEC-Na safety simulation code” *Proceedings of ICAPP 2015* Nice (France) May 3-6, 2015 15072
3. G. Bandini et al “Status of validation of ASTEC-Na sodium thermal-hydraulic models” *JASMIN-MODELLING-D2.5*. 2013
4. L. E. Herranz et al “Development and Validation of ASTEC-Na Thermal-Hydraulic Models”, *Proceedings of the 40th Annual Meeting of the SNE*, Valencia, Spain, 1-3 October 2014.
5. G. Bandini et al “Pre-test analyses for the experimental sodium loop KASOLA with ASTEC-Na and benchmarking with other codes” *Proceedings of ICAPP 2015* Nice (France) May 3-6, 2015, 15222
6. G. Brillant, L. Laborde. “Sodium thermalhydraulics in ASTEC/CESAR” *Confidential Rapport n. PSN-RES/SAG/2014-00008* 2014
7. N. Trégourès, A. Moal, “ASTEC V1 code: CESAR physical and numerical modeling”. *Confidential Rapport IRSN/SEMAC/2006/188*. 2006
8. J.R.S. Thom et al. *Symposium on Boiling Heat Transfer in Steam Generating Units and Heat Exchangers*, Manchester, 15-16 September 1965. 1965
9. H.J. Ivey, D.J. Morris. “On the relevance of the vapor-liquid exchange mechanism for subcooled boiling heat transfer at high pressure”. *Technical Report AEEW-R137, UKAEA* ., 1962
10. P.J. Berenson “Film boiling heat transfer from a horizontal surface” *J. Heat Trans. (ASME)*, 83:351–358. 1961
11. H. K. Forster, N. Zuber. „Bubble dynamics and boiling heat transfer” *AIChE J.*, 1:532–535. 1955
12. F.P. Incropera, D-P. “Fundamentals of Heat and Mass Transfer”. Ch. 8. John Wiley & Sons. 2001
13. RELAP5-3D© Code Development Team, “RELAP5-3D© code manual volume I: code structure, system models, and solution methods”, *Idaho National Laboratory Report INEEL-EXT-98-00834*, rev. 4.0, Idaho Falls, Idaho, USA, June 2005.
14. C. D. Fletcher, R. R. Schultz, “RELAP5/MOD3 Code Manual”, *NUREG/CR-5535, INEL-95/0174*, Idaho National Engineering Laboratory, June 1995.
15. G. Geffraye et al., “CATHARE 2 V2.5_2: A single version for various applications”, *Nuclear Engineering and Design* 241 (2011) 4456-4463.
16. U. Imke, D. Struwe, et al. “Status of the SAS4A-code development for consequence analysis of core disruptive accidents” *Proceedings of an International Topical Meeting. Sodium Cooled Fast Reactor Safety*. 2-232. Obninsk, Russia, October 1994
17. JAEA “A SAS4A Study on the ULOF Initiating Phase Energetics of the Fast Breeder Reactor (FBR)”. *JNES/FBRG10-004. Japan Nuclear Energy Safety Organization (JNES)* Feb. 2011